Laboratory Assessment of Rubber Grids Reinforced Ballast under Impact Testing

Anees Raja Siddiqui

PhD student, Transport Research Centre, School of Civil and Environmental Engineering, University of Technology Sydney, Ultimo, Sydney, Australia; and ARC Industrial Transformation Training Centre for Advanced Technologies in Rail Track Infrastructure (ITTC-Rail).

Buddhima Indraratna, PhD (Alberta), FTSE, FIEAust, FASCE, FGS

Distinguished Professor of Civil Engineering and Director of Transport Research Centre, University of Technology Sydney, Ultimo, Australia; Founding Director, ARC Industrial Transformation Training Centre for Advanced Technologies in Rail Track Infrastructure (ITTC-Rail)

Trung Ngo, PhD, MASCE

Senior lecturer, Transport Research Centre, School of Civil and Environmental Engineering, University of Technology Sydney, Ultimo, Australia.

Cholachat Rujikiatkamjorn, PhD, MASCE

Professor, Transport Research Centre School of Civil and Environmental Engineering, University of Technology Sydney, Ultimo, NSW 2007, Australia

Technical Note, Submitted to Géotechnique

Author for correspondence:

Distinguished Professor Buddhima Indraratna

Transport Research Centre

University of Technology Sydney

Ultimo, NSW 2007

Australia.

Ph: +61 2 9514 8000

Email: buddhima.indraratna@uts.edu.au

Laboratory Assessment of Rubber Grids Reinforced Ballast under Impact Testing

Authors: Anees Raja Siddiqui[a], Buddhima Indraratna[b], Trung Ngo[c], and Cholachat Rujikiatkamjorn[d]

[a]PhD student, Transport Research Centre, School of Civil and Environmental Engineering, University of Technology Sydney, Ultimo, Sydney, Australia; and ARC Industrial Transformation Training Centre for Advanced Technologies in Rail Track Infrastructure (ITTC-Rail). Email: aneesraja.siddiqui@student.uts.edu.au

[b]Distinguished Professor of Civil Engineering and Director of Transport Research Centre, University of Technology Sydney, Ultimo, Australia; Founding Director, ARC Industrial Transformation Training Centre for Advanced Technologies in Rail Track Infrastructure (ITTC-Rail). Email: buddhima.indraratna@uts.edu.au

[c]Senior lecturer, Transport Research Centre, School of Civil and Environmental Engineering, University of Technology Sydney, Ultimo, Australia; Email: Trung.Ngo@uts.edu.au

[d]Professor, Transport Research Centre School of Civil and Environmental Engineering, University of Technology Sydney, Ultimo, NSW 2007, Australia; Email: Cholachat.Rujikiatkamjorn@uts.edu.au

Abstract: This paper presents a study on the use of rubber grids fabricated from end-of-life conveyor belts (i.e., discarded from the mining industry) to improve the performance of ballast tracks. The square apertures of these recycled rubber sheets were cast using a waterjet cutting process. A series of large-scale impact tests were performed on ballast specimens stabilised with three different grids of varied effective area ratios ($K_{A.eff}$) to evaluate their effectiveness in mitigating the applied impact forces, in relation to both displacement and breakage of the ballast aggregates. *Smart Ballast* particles with motion-sensing capabilities were adopted to monitor the interaction between the grid and ballast assembly. The impact test results indicate that the inclusion of a rubber grid decreases the deformation and breakage of ballast as well as reduces its vibrations. This study demonstrates that these recycled rubber grids with optimum effective area ratios can be more effective than conventional polymer geogrids, apart from the obvious environmental benefits.

Keywords: *Granular materials, Impact testing, Railway tracks, Rubber grids, Smart ballast, Sustainability.*

INTRODUCTION

Ballasted tracks are the primary means of freight and passenger transport in Australia, having a network of more than 35,000 km (Indraratna et al. 2011). With increasing train speeds and axle loads, inevitable track deterioration leads to increased annual maintenance costs (RailCorp 2020). Moreover, track imperfections cause impact forces and consequential noise and vibrations (Suiker et al. 2005, Nimbalkar et al. 2012, Remennikov and Kaewunruen 2014). In particular, impact loads are usually generated by: (i) track transitions such as bridge approaches, road crossings, and turnouts (Shan et al. 2020, Xin et al. 2020, Jing et al. 2022); and (ii) rail abnormalities such as wheel-flat and dipped rails, which can be dangerous and impede the efficiency and safety of rail tracks (Powrie et al. 2007, Insa et al. 2014, Le Pen et al. 2016, Indraratna et al. 2019, Varandas et al. 2020).

Previous studies have demonstrated the advantages of polymer geogrids under repeated train loading in reinforcing and restraining ballast aggregates from lateral displacement (e.g. Bathurst and Raymond 1987, Brown et al. 2007, Tutumluer et al. 2012, Dhanya et al. 2019, Sweta and Hussaini 2022). However, at transition zones (e.g., concrete bridge decks or level crossings), traditional polymeric geogrids would not be able to effectively impede the adverse effects of impact loads (Miri et al. 2022, Chen and McDowell 2016). In such situations, extensive ballast degradation (breakage) may occur as reported by Indraratna et al. (2014).

End-of-life rubber conveyor belts are a major source of rubber waste that can cause safety and environmental concerns (Leong et al. 2022, Nuzaimah et al. 2018). They are made from a blend of natural and synthetic rubber and are strong and durable enough to move heavy materials (Sol-Sánchez et al. 2015, Sienkiewicz et al. 2017, Indraratna et al. 2019), hence their re-fabrication to be placed as grids in ballast rail tracks is attractive both from technical and circular economy perspectives. Furthermore, the addition of rubber components in track ballast has demonstrated beneficial effects including reduced particle breakage and improved stress conditions (Guo et al. 2019, Guo et al 2022). This study used recycled conveyor belts to make rubber grids (RGs) with different geometric configurations and tested their effectiveness in a ballast assembly under impact loading. With regard to improved track stability, these recycled grids serve two main purposes: (i) through enhanced damping, they are able to withstand cyclic and impact loads generated by moving trains, thus minimising ballast degradation; (ii) they provide a mechanical interlock with ballast aggregates to prevent lateral spreading.

LARGE-SCALE IMPACT TESTS

Materials tested

Fresh latite basalt (volcanic) produced from quarries located south of Sydney is highly angular in shape. In this study, these aggregates were thoroughly washed and dried before being sieved and mixed according to the current Australian standards (AS: 2758.7: 2015), as shown in Figure 1a. The apertures on the rubber grids were made using high precision waterjet cutting as shown in Figure 1b. Compressive and tensile tests were also performed on the rubber panel (Fig. 1c), and the relevant mechanical properties are given in Table 1.

Based on previous findings by Indraratna et al. (2012) in relation to the effect of aperture size on the interface shear strength, three different rubber grids, RG-S1, RG-S2, and RG-S3, were prepared with the same aperture size of 51×51 mm, but varying the effective area ratios ($K_{A.eff}$) and the rib thicknesses. The effective area ratio ($K_{A.eff}$) can be defined as the ratio of an effective area to the total area of the grid:

$$K_{A.eff} = \frac{(B-t)(L-t)-S}{(B-t)(L-t)} \quad (1)$$

where, $S = \sum A^2$, A is the area of an aperture, and B, L and t are geometric parameters of the rubber grid (Fig. 1b). The geometric details of the rubber grids are presented in Table 2. The role of the effective area ratio when subjected to high impact loading is imperative when considering the performance of these recycled rubber grids placed in ballasted tracks.

Impact testing facility and sample preparation

A high-capacity drop weight impact testing apparatus had a free-fall hammer with a weight of 5.81 kN that could be dropped from a height of up to 6 m with a maximum drop velocity of 10 m/s (Remennikov and Kaewunruen 2014). The impact testing equipment and the schematic representation of a typical ballast sample used for laboratory testing are shown in Figure 2a. A load cell was attached to the drop hammer, and a piezoelectric accelerometer was mounted on the top surface of the specimen assembly to measure the impact load and acceleration during testing. These instruments were connected to a computer-controlled automated data acquisition system (Fig. 2b). The hammer was mechanically raised to a specified drop height (h_d) and then released by an electronic control system to drop it onto the test specimen.

The ballast test specimen (300 mm in diameter and 500 mm high) was prepared and compacted in a cylindrical rubber membrane (7 mm thick). A 50 mm steel plate was placed at the bottom of the test specimen, followed by a 100 mm thick capping layer (sand and gravel mixture) compacted to a unit weight of 20.5 kN/m^3. On top of the capping layer, a layer of rubber grid was positioned, followed by a 350 mm thick layer of ballast (Fig. 2c). The ballast was placed in three equal sub-layers and compacted to the desired bulk unit weight of 15.3 kN/m^3, using a hand-held vibratory hammer. It is noted that this is similar to the initial density in most Australian tracks, where over-compaction during tamping is avoided to prevent breakage (Indraratna et al, 2011). Transport for NSW (2018) recommends a bulk unit weight of at least 1400 kg/m^3 for ballast after initial tamping, which is easily achieved in our laboratory tests. A steel plate (50 mm) was placed on the top of the ballast layer to distribute the load applied by the drop hammer. Two halves of a rigid steel mould supported the rubber cell membrane during the compaction process so that the diameter of the specimen remained consistent (300 mm) throughout its height.

A *Smart Ballast* wireless device was employed to monitor ballast particle rotation during impact tests (Siddiqui et al. 2021). A high-precision 3D rotary scanner was used to accurately capture the geometry and surface roughness of an actual ballast particle. Using this information, *Smart Ballast* particle was 3D printed using a plastic filament infused with metal and had the same density as ballast. A wireless motion sensor was embedded in that particle which tracked its accelerations and rotation angles via Bluetooth. This device was an improvement over previous devices (Liu et al. 2017, Zeng et al. 2019, and Fu et al. 2020) because it accurately captured the density and shape of a realistic ballast.

This study involved four impact tests with and without rubber grids, and the testing configuration and program are summarised in Table 2. It has been observed that impact loads on Australian railway tracks primarily occur in areas where there are rail corrugations and significant wear on the wheels, in addition to locations of transition zones. To generate dynamic stresses representing typical impact forces measured in the field (Indraratna et al. 2014), a hammer was dropped from a predetermined height (h_d) of 150 mm, and each test was subjected to 12 hammer drops (N=12) as previous studies by Nimbalkar et al. (2012) and Indraratna et al. (2020) showed that after 10 hammer drops, the increase in deformation of ballast specimens was not significant. Therefore, the testing program in this study followed the same methodology which also allowed for valuable comparative analysis. The height of the specimen and its circumference at three different locations (bottom, top and middle) were measured after each drop to determine the vertical and average lateral deformation. Subsequently, the ballast was sieved and weighed to quantify the amount of breakage.

RESULTS AND DISCUSSIONS

Impact forces

Figure 3 shows the comparison of impact forces of unreinforced ballast specimen with RGs and a conventional polymer geogrid during the first 0.3 seconds at the 12th drop. Two distinct force peaks were observed under impact loads: multiple sharp force peaks (P_1), followed by smaller and more gradual forces (P_2). The inertia of the top-loading plate caused sharp peaks (P_1) as it resisted the downward motion of the hammer occurring in a relatively short time with an amplitude ranging from 345 kN to 410 kN. In contrast, the force (P_2) was of much lower magnitude but lasted longer than P_1, reaching a stable value of around 50–75 kN.

The beneficial effect of rubber grids in reducing impact forces is demonstrated in Figure 4, summarising the variations of measured impact loads, P_1 and P_2 and cumulative impact energy. By applying the principle of energy conservation, the total impact energy resulting from one drop of a 5.81 kN hammer from a height of 150 mm was calculated to be 0.87 kJ. When subjected to 12 hammer drops, the total accumulated impact energy was determined to be slightly greater than 10 kJ. In general, the P_1 and P_2 forces show a gradual increase throughout the subsequent impact drops due to the densification of the ballast assembly, except the polymer geogrid-ballast showing some random fluctuation in P_1 (Fig. 4a). The inclusion of rubber grids generally decreases the magnitude of impact force. Indeed, compared to unreinforced ballast (maximum P_1 and P_2 are 387 kN, 83 kN, respectively), the RG-S2 provides the highest reduction in P_1 and P_2 (maximum P_1 and P_2: 292 kN, 68 kN, respectively), while the RG-S1 provides only a marginal reduction in impact forces (maximum P_1 and P_2: 365 kN, 76 kN, respectively). In contrast to the damping offered by the rubber grids, the inclusion of a conventional polymer geogrid carried out in an independent study (Indraratna et al.2020) does not reduce impact force but instead increases the maximum P_1 force to 427 kN (Fig. 4a) and maximum P_2 force to 87 kN (Fig. 4b).

Ballast deformation

The measured axial (ε_a) and radial (lateral) strains (ε_r) are shown in Figures 5a & 5b, and the corresponding shear strain (ε_s) and volumetric strain (ε_v) are presented in Figures 5c & 5d. The radial strain was calculated as the average of the circumferential strains measured at three different heights of the sample (bottom, middle, and top). The volumetric strain was calculated as the change in volume divided by the initial volume of the sample. With increasing N, all tests consistently demonstrate increased axial and radial strains when ballast aggregates are compressed vertically and displaced laterally. Compared to unreinforced ballast, tests with the inclusion of RG resulted in decreased axial and lateral strains. After the 9th drop, the deformation of ballast becomes more gradual towards the end of the test. The most significant reduction in deformation occurred when the rubber grid, RG-S2 was used (up to 30.8% for axial strain and 20.9% for radial strain), followed by RG-S3 (28.5% for axial strain and 16.4% for radial strain) and RG-S1 (13.6% for axial strain, while unnoticeable change for radial strain). The inclusion of polymer geogrid marginally decreases ballast deformation (only 4.5% and 5.7% for axial and radial strain, respectively). In general, both the volumetric and shear strains increase following a similar trend to the axial strain, as the ballast aggregates tend to initially compress rapidly, and then show a diminishing rate of straining after the 9th drop upon particle rearrangement. However, the shear and volumetric strains significantly decrease (by 20 to 35%) with rubber grids due to the damping of rubber. In contrast, the improvement was relatively less noticeable (only 3.7%) with a conventional polymer geogrid that is relatively stiff and incapable of absorbing impact energy. Further, it was observed that RG-S2 provided the best effective area ratio for minimising impact-induced deformation of ballast as it optimises the combined benefit of rubber grids through enhanced damping and providing a better mechanical interlock with ballast aggregates. It is worth mentioning that the effective area ratio alone does not play an absolute role in the performance of these grids, because, in theory, an effective area ratio of 1 would provide maximum damping but it will not have any reinforcement effect.

Ballast breakage

After each impact test, ballast was sieved to determine any changes in gradation and associated breakage using the ballast breakage index (*BBI*) introduced by Indraratna et al. (2005), as shown in Figure 6a. Figure 6b shows measured BBI for different tests and corresponding reduced breakage (R_{BBI}). The percentage reduction in the ballast breakage index (R_{BBI}) attributed to the inclusion of the rubber grids is determined as:

$$R_{BBI}(\%) = \frac{BBI_{No\_RG} - BBI_{With\_RG}}{BBI_{No\_RG}} \quad (2)$$

where, BBI_{No_RG} and $BBI_{With\_ RG}$ are the measured ballast breakage index for unreinforced and rubber grid-reinforced ballast assemblies, respectively. A summary of ballast particle size distributions after each test and the corresponding measured *BBI* and R_{BBI} are presented in Table 3.

Measured breakage data show that the rubber grids cause a significant reduction in ballast breakage. Indeed, the *BBI* of unreinforced ballast is 0.215, while the tests with the RG-S1, RG-S2 and RG-S3 indicate levels of *BBI* as 0.172, 0.141 and 0.135, respectively. The rubber grids RG-S2 and RG-S3 provide the most significant reduction in breakage, achieving R_{BBI} of up to 30.7% and 32.8%, respectively, while the tests with RG-S1 and conventional geogrid show R_{BBI} of 14.6% and 29.9%, respectively. These test results demonstrate that the amount of ballast breakage is significantly reduced by the addition of rubber grids which can be attributed to the damping property (i.e., energy-absorbing nature); in other words, less impact energy is transferred to the ballast layer leading to reduced degradation. It is noteworthy that ballast degradation and energy consumption are not always directly related due to variations in ballast quality between samples. Other factors such as microcracks and mineralogical composition, as well as the type of track inclusions and fouling in track beds, can also influence particle breakage.

Rotation of a Smart Ballast

Figure 7a shows the evolution of rotation angles in the *x* and *y* directions as obtained via *Smart Ballast* at different impact drops for the tests with and without a rubber grid (RG-S2). The visualisation of a *Smart Ballast* particle in three-dimensional orientation illustrating how it changes during the impact test is also presented in Figure 7b. The results show that the unreinforced particle has undergone a sudden change in its orientation during the initial hammer drops, which can be attributed to the compression and re-arrangement of ballast under impact forces. The rotation angles θ_x and θ_y change from 0° to about 60° and 55°, respectively. In contrast, the inclusion of RG-S2 provided the most effective interlock to the *Smart Ballast* particle by reducing its rotation significantly, as its final θ_x and θ_y were only around 6° and 5°, respectively. This observation practically proves that the rubber grid could provide a non-displacement boundary in the ballast through an effective interlock that confines and prevents the ballast particles from rotating.

Acceleration responses

Figure 8 compares acceleration responses measured at the 12th drop. The maximum acceleration for unreinforced ballast was 177 g, while those measured for the RG-S1, RG-S2 and RG-S3 were about 128 g, 110 g and 109 g, demonstrating a 27.5%, 37.6% and 38.4% reduction in peak acceleration, respectively. Not surprisingly, the inclusion of a conventional polymer geogrid did not reduce vibration. Acting like a shock absorber, placing rubber grids underneath the ballast layer can reduce the maximum (peak) accelerations and enable vibration attenuation of the assemblies.

CONCLUSIONS

The performance of recycled rubber grids as ballast reinforcement was evaluated using a large-scale impact testing facility. Four large-scale impact tests involving twelve hammer drops were conducted with and without the rubber grids. The results of different rubber grids were compared to those of unreinforced ballast and a conventional polymer geogrid in terms of impact forces, ballast deformation, degradation (breakage), and vibrations. Based on the test results, following are the conclusions of this study.

- The impact forces (P_1 and P_2) significantly decreased when rubber grids were placed beneath the ballast. Compared to the unreinforced specimen, RG-S2 provided the greatest reduction in P_1 and P_2 (by 24.5% and 18%, respectively), while RG-S1 only had a slight reduction.
- Rubber grids significantly decreased ballast deformation, with the highest reduction when RG-S2 was used (30.8% for axial strain and 20.9% for radial strain). The corresponding shear and volumetric strains also decreased by 20% to 35%.
- Rubber grids greatly reduced ballast breakage during impact testing, with RG-S2 and RG-S3 causing a reduction in breakage of 30.7% and 32.8%, respectively.
- Rubber grids provided an effective interlock to the ballast particles, as their rotation angles, measured through *Smart Ballast*, significantly decreased.
- Rubber grids showed a significant reduction in ballast aggregate vibrations, with RG-S1, RG-S2, and RG-S3 showing reductions of 27.5%, 37.6%, and 38.4%, respectively.

ACKNOWLEDGMENT

This study was conducted under the auspices of the Industrial Transformation Training Centre for Advanced Technologies in Rail Track Infrastructure (ITTC-Rail), c/o Australian Research Council (ARC-IC170100006), and Discovery Project (DP220102862). The authors gratefully appreciate the close collaborations with Bridgestone Corp. (c/o Dr Endo Shigeki) and Sydney

Trains (Transport for NSW) for valuable inputs and help throughout the project. The authors are also thankful to the technical staff at the University of Wollongong (c/o Mr Cameron Neilson and Mr Jordan Wallace) for their assistance during the experimental program amidst COVID-19 restrictions.

REFERENCES

AS 2758.7: (2015). Aggregates and rock for engineering purposes, Part 7. *Railway Ballast. Standard Australia* NSW, Australia.

ASTM D412-16. (2021). American Society for Testing and Materials. Standard Test Methods for Vulcanized Rubber and Thermoplastic Elastomers--tension. ASTM international.

ASTM D575-91. (2018). American Society for Testing and Materials. Standard test methods for rubber properties in compression. ASTM International.

AS 1333 (2019). Standards Australia. Conveyor belting of elastomeric and steel cord construction (Reconfirmed 2019)

ASTM D2240-15 (2021). American Society for Testing and Materials. (2021). Standard test method for rubber property-Durometer hardness. ASTM International.

Bathurst, R. J. and Raymond, G. P. (1987). Geogrid reinforcement of ballasted track. *Transportation Research Record* 1153: 8-14.

Brown, S. F., Kwan, J. and Thom, N. H. (2007). Identifying the key parameters that influence geogrid reinforcement of railway ballast. *Geotextiles and Geomembranes* 25(6): 326-335.

Chen, C. and McDowell, G. R. (2016). An investigation of the dynamic behaviour of track transition zones using discrete element modelling. *Proceedings of the Institution of Mechanical Engineers, Part F: Journal of Rail and Rapid Transit* 230(1): 117-128.

Dhanya, J. S., Boominathan, A. and Banerjee, S. (2019). Performance of Geo-Base Isolation System with Geogrid Reinforcement. *International Journal of Geomechanics* 19(7): 04019073.

Esveld, C. (2014). Modern railway track, MRT Press, The Netherlands.

Fu, L., Tian, Z., Zhou, S., Zheng, Y. and Wang, B. (2020). Characterisation of ballast particle's movement associated with loading cycle, magnitude and frequency using SmartRock sensors. *Granular Matter* 22(3): 63 (1-13).

Gładysiewicz, L., Konieczna-Fuławka, M., & Woźniak, D. (2019). Determining of damping factor of belt on the basis of hysteresis loop in calculation of conveyor belt rolling resistance. International Multidisciplinary Scientific GeoConference : SGEM, 19(1.3), 209–216.

Gu, Q., Zhao, C., Bian, X., Morrissey, J. P. and Ooi, J. Y. (2022). Trackbed settlement and associated ballast degradation due to repeated train moving loads. *Soil Dynamics and Earthquake Engineering* 153: 107109.

Guo, Y., Shi, C., Zhao, C., Markine, V. and Jing, G., 2022. Numerical analysis of train-track-subgrade dynamic performance with crumb rubber in ballast layer. Construction and Building Materials, 336, p.127559.

Guo, Y., Markine, V., Qiang, W., Zhang, H. and Jing, G., 2019. Effects of crumb rubber size and percentage on degradation reduction of railway ballast. Construction and Building Materials, 212, pp.210-224.

Indraratna, B., Babar Sajjad, M., Ngo, T., Gomes Correia, A. and Kelly, R. (2019). Improved performance of ballasted tracks at transition zones: A review of experimental and modelling approaches. *Transportation Geotechnics* 21: 100260.

Indraratna, B., Lackenby, J. and Christie, D. (2005). Effect of confining pressure on the degradation of ballast under cyclic loading. *Géotechnique* 55(4): 325–328.

Indraratna, B., Ngo, T., Bessa Ferreira, F., Rujikiatkamjorn, C. and Shahkolahi, A. (2020). Laboratory examination of ballast deformation and degradation under impact loads with synthetic inclusions. *Transportation Geotechnics* 25: 100406.

Indraratna, B., Nimbalkar, S. and Neville, T. (2014). Performance assessment of reinforced ballasted rail track. *Proceedings of the Institution of Civil Engineers - Ground Improvement* 167(1): 24-34.

Indraratna, B., Qi, Y., Ngo, T. N., Rujikiatkamjorn, C., Neville, T., Ferreira, F. B. and Shahkolahi, A. (2019). Use of geogrids and recycled rubber in railroad infrastructure for enhanced performance. *Geosciences* 9(1): 1-26.

Indraratna, B., Salim, W. and Rujikiatkamjorn, C. (2011). Advanced Rail Geotechnology - Ballasted Track, CRC Press, Taylor & Francis Group, London, UK.

Indraratna, B., Hussaini, S. K. K. and Vinod, J. S. (2012). On the shear behavior of ballast-geosynthetic interfaces. Geotechnical Testing Journal 35(2): 305-312.

Insa, R., Salvador, P., Inarejos, J. and Medina, L. (2014). Analysis of the performance of under-sleeper pads in high-speed line transition zones. *Proceedings of the Institution of Civil Engineers-Transport* 167(2): 63-77.

Jing, G., Siahkouhi, M., Wang, H. and Esmaeili, M. (2022). The improvement of the dynamic behavior of railway bridge transition zone using furnace slag reinforcement: A numerical and experimental study. *Proceedings of the Institution of Mechanical Engineers. Part F, Journal of rail and rapid transit* 236(4): 362-374.

Le Pen, L., Milne, D., Thompson, D. and Powrie, W. (2016). Evaluating railway track support stiffness from trackside measurements in the absence of wheel load data. *Canadian Geotechnical Journal* 53(7): 1156-1166.

Leong, S.-Y., Lee, S.-Y., Koh, T.-Y. and Ang, D. T.-C. (2022). 4R of rubber waste management: current and outlook. *Journal of Material Cycles and Waste Management*.

Liu, S., Huang, H., Qiu, T. and Gao, L. (2017). Comparison of Laboratory Testing Using SmartRock and Discrete Element Modeling of Ballast Particle Movement. *Journal of Materials in Civil Engineering* 29(3): D6016001.

Miri, A., Zakeri, J. A., Thambiratnam, D. P. and Chan, T. H. T. (2022). Mitigation of track buckling in transition zones of steel bridges by geotextile reinforcement of the ballast layer. *Geotextiles and Geomembranes* 50(2): 282-292.

Nimbalkar, S., Indraratna, B., Dash, S. K. and Christie, D. (2012). Improved Performance of Railway Ballast under Impact Loads Using Shock Mats. *Journal of Geotechnical and Geoenvironmental Engineering* 138(3): 281-294.

Nuzaimah, M., Sapuan, S., Nadlene, R. and Jawaid, M. (2018). Recycling of waste rubber as fillers: A review. *IOP Conference Series: Materials Science and Engineering* 368(1): 012016.

Powrie, W., Yang, L. A. and Clayton, C. R. I. (2007). Stress changes in the ground below ballasted railway track during train passage. *Proceedings of the Institution of Mechanical Engineers: Part F: Journal of Rail and Rapid Transit*: 247-261.

RailCorp. (2020). Annual report 2019-20. Transport Asset Holding Entity of New South Wales, Australia.

Remennikov, A. M. and Kaewunruen, S. (2014). Experimental load rating of aged railway concrete sleepers. *Engineering Structures* 76: 147-162.

Shan, Y., Zhou, S., Wang, B. and Ho, C. L. (2020). Differential Settlement Prediction of Ballasted Tracks in Bridge-Embankment Transition Zones. *Journal of Geotechnical and Geoenvironmental Engineering* 146(9): 04020075.

Siddiqui, A. R., Indraratna. B. and Ngo, T. (2021). Developing Realistic "Smart Ballast" for Improved Understanding of Ballasted Tracks – A conceptual Design. *Proceedings of the International Conference on Geotechnical Engineering ICGE Colombo 2020*: 73-76.

Sienkiewicz, M., Janik, H., Borzędowska-Labuda, K. and Kucińska-Lipka, J. (2017). Environmentally friendly polymer-rubber composites obtained from waste tyres: A review. *Journal of cleaner production* 147(2017): 560-571.

Sol-Sánchez, M., Moreno-Navarro, F. and Rubio-Gámez, M. C. (2015). The use of elastic elements in railway tracks: A state of the art review. *Construction and Building Materials* 75: 293-305.

Suiker, A. S. J., Selig, E. T. and Frenkel, R. (2005). Static and cyclic triaxial testing of ballast and subballast. *Journal of Geotechnical and Geoenvironmental Engineering, ASCE* 131(6): 771–782.

Sweta, K. and Hussaini, S. K. K. (2022). Role of particle breakage on damping, resiliency and service life of geogrid-reinforced ballasted tracks. *Transportation Geotechnics* 37: 100828.

Transport for NSW, (2018). Technical Note – T HR TR 00192 ST: Ballast, version 2, Issued date: 03 July 2018.

Tutumluer, E., Huang, H. and Bian, X. (2012). Geogrid-aggregate interlock mechanism investigated through aggregate imaging-based discrete element modeling approach. *International Journal of Geomechanics* 12(4): 391-398.

Varandas, J. N., Paixão, A., Fortunato, E., Zuada Coelho, B. and Hölscher, P. (2020). Long-term deformation of railway tracks considering train-track interaction and non-linear resilient behaviour of aggregates – a 3D FEM implementation. *Computers and Geotechnics* 126: 103712.

Xin, T., Ding, Y., Wang, P. and Gao, L. (2020). Application of rubber mats in transition zone between two different slab tracks in high-speed railway. *Construction and Building Materials* 243: 118219.

Zeng, K., Qiu, T., Bian, X., Xiao, M. and Huang, H. (2019). Identification of ballast condition using SmartRock and pattern recognition. *Construction and Building Materials* 221: 50-59.

Table 1. Engineering and mechanical properties of rubber panels

Properties	Values	Unit	Standard
Thickness	10 - 11	mm	—
Density	1.10	g/cc	—
Tensile strength at 2% strain	80	kPa	ASTM D412
Tensile strength at 5% strain	180	kPa	ASTM D412
Compressive strength at 2% strain	100	kPa	ASTM D575
Compressive strength at 5% strain	750	kPa	ASTM D575
Abrasion resistance	81	mm^3	AS 1333
Hardness	60	-	ASTM D2240
Modulus of Elasticity (E)	4	MPa	-
Damping Factor (ψ)	0.35	-	Gładysiewicz et al. (2019)

Table 2. Summary of impact testing program and rubber grids (RGs) used in the tests

Test No.	Test Configuration	Aperture Shape	Aperture Size (mm)	Rib Thickness (mm)	Effective Area Ratio ($K_{A.eff}$)	Grid Geometry
1	Unreinforced Ballast	-	-	-	-	-
2	RG-S1	Square	51×51	7.4	0.4	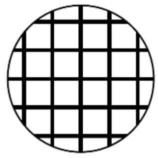
3	RG-S2	Square	51×51	10.6	0.5	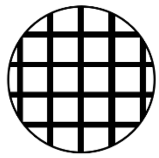
4	RG-S3	Square	51×51	14.8	0.6	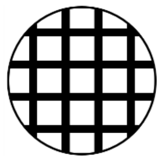

Table 3. Particle size gradation of ballast before & after test conducted in this study

Sieve Size (mm)	Percentage Passing (%)				
	Initial gradation before test	Unreinforced ballast	With RG-S1	With RG-S2	With RG-S3
63	100.0	100.0	100.0	100.0	100.0
53	100.0	100.0	100.0	100.0	100.0
37.5	60.0	63.9	62.3	61.3	62.7
26.5	30.0	32.3	32.7	31.6	32.0
19	13.0	14.6	15.1	16.6	13.3
13.2	5.0	5.5	6.2	6.2	5.5
9.5	0.0	0.7	0.4	0.3	0.4
4.75	0.0	0.0	0.0	0.00	0.0
2.36	0.0	0.0	0.0	0.00	0.0
Measured BBI		**0.215**	**0.172**	**0.141**	**0.135**
Reduction in breakage (%)		**-**	**14.6**	**30.7**	**32.8**

Figure Captions

Figure 1. (a) Particle size distributions of ballast and capping, (b) Preparing rubber grids from rubber panel using waterjet cutting; (c) Compression and tensile tests of rubber panel

Figure 2. (a) Large-scale impact testing facility and sample preparation; (b) Data acquisition system; and (c) sample preparation

Figure 3. Comparison of impact forces of unreinforced ballast specimen with: (a) rubber grid RG-S1; (b) RG-S2; (c) RG-S3; and (d) conventional polymer geogrid.

Figure 4. Variations of measured impact loads, (a) P_1 and (b) P_2 at a different number of hammer drops.

Figure 5. Measured deformation of ballast with the inclusion of rubber grids: (a) vertical strain, (b) lateral strain; (c) shear strain; and (d) volumetric strain.

Figure 6. (a) Determination of Ballast Breakage Index (BBI), and (b) Measured ballast breakage with the inclusion of different rubber grids in comparison with a conventional polymer geogrid

Figure 7. (a) Measured rotation of *Smart Ballast* during the impact tests and (b) Movements of the *Smart Ballast* captured at varying drops

Figure 8. Measured acceleration of ballast with the inclusion of grids: (a) RG-S1; (b) RG-S2; (c) RG-S3; and (d) conventional polymer geogrid

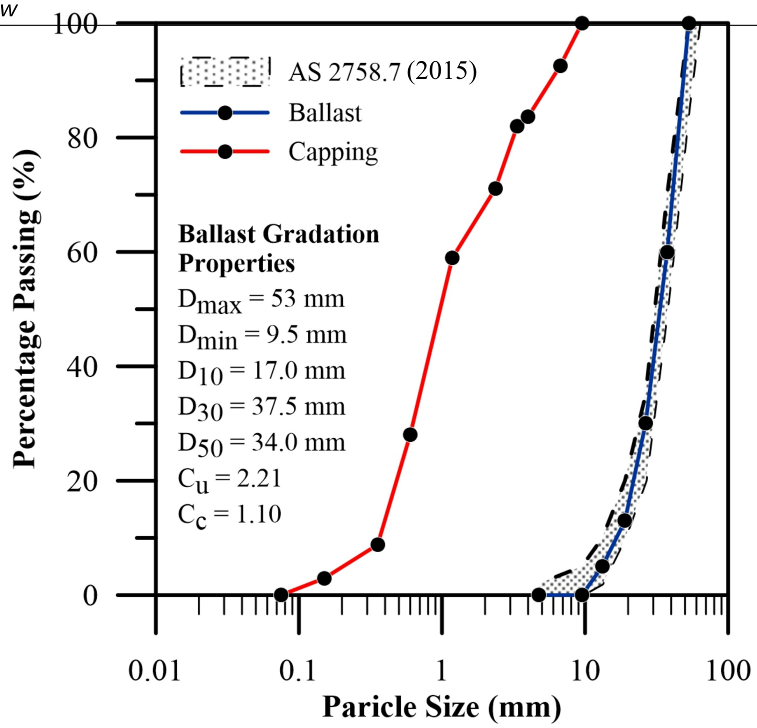
AS 2758.7 (2015)
Ballast
Capping
Ballast Gradation Properties
Dmax = 53 mm
Dmin = 9.5 mm
D10 = 17.0 mm
D30 = 37.5 mm
D50 = 34.0 mm
Cu = 2.21
Cc = 1.10
Percentage Passing (%)
Paricle Size (mm)
0.01
0.1
1
10
100
0
20
40
60
80
100

(a)

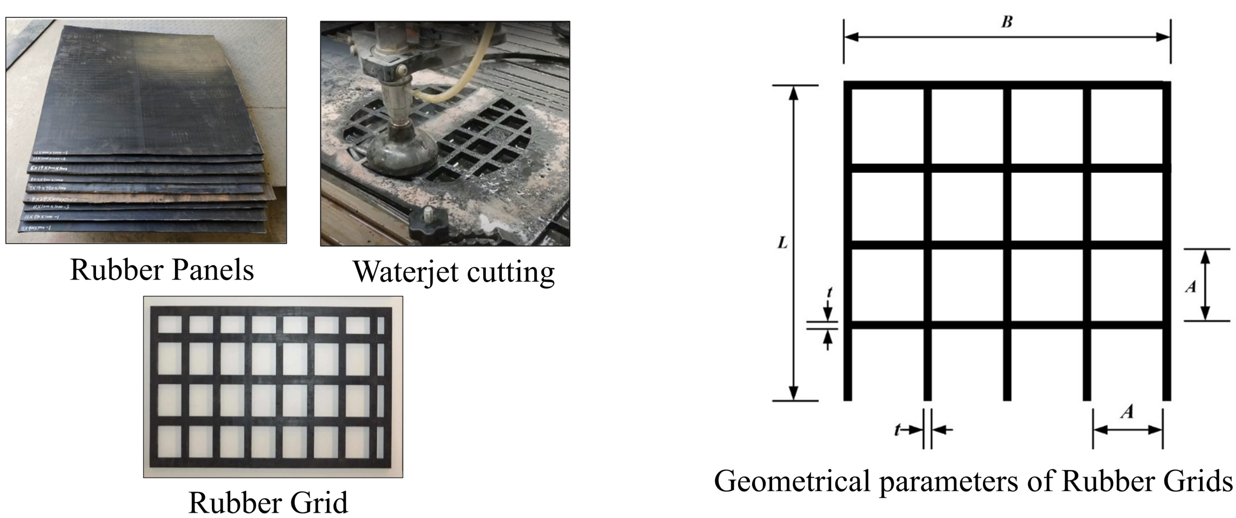
Rubber Panels
Waterjet cutting
Rubber Grid
B
L
t
A
Geometrical parameters of Rubber Grids

(b)

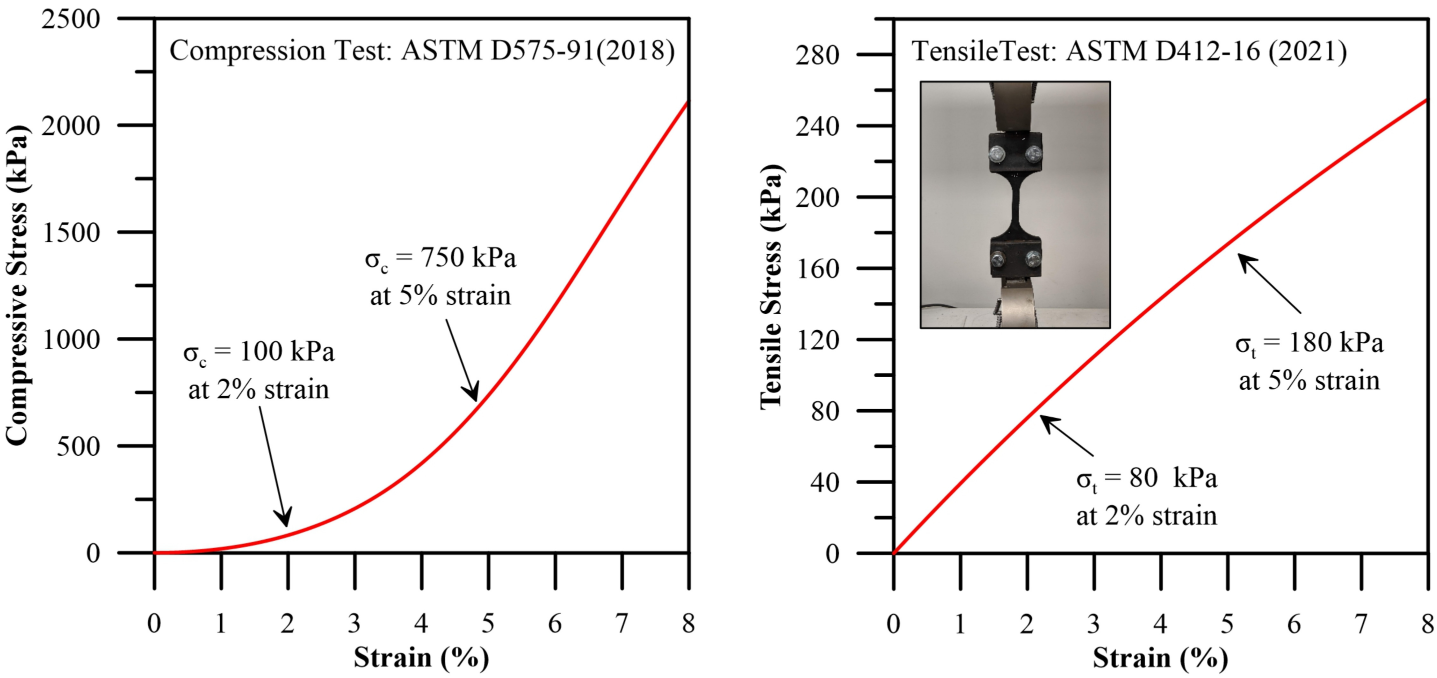
Compression Test: ASTM D575-91(2018)
σc = 750 kPa
at 5% strain
σc = 100 kPa
at 2% strain
Compressive Stress (kPa)
Strain (%)
TensileTest: ASTM D412-16 (2021)
σt = 180 kPa
at 5% strain
σt = 80 kPa
at 2% strain
Tensile Stress (kPa)
Strain (%)

(c)

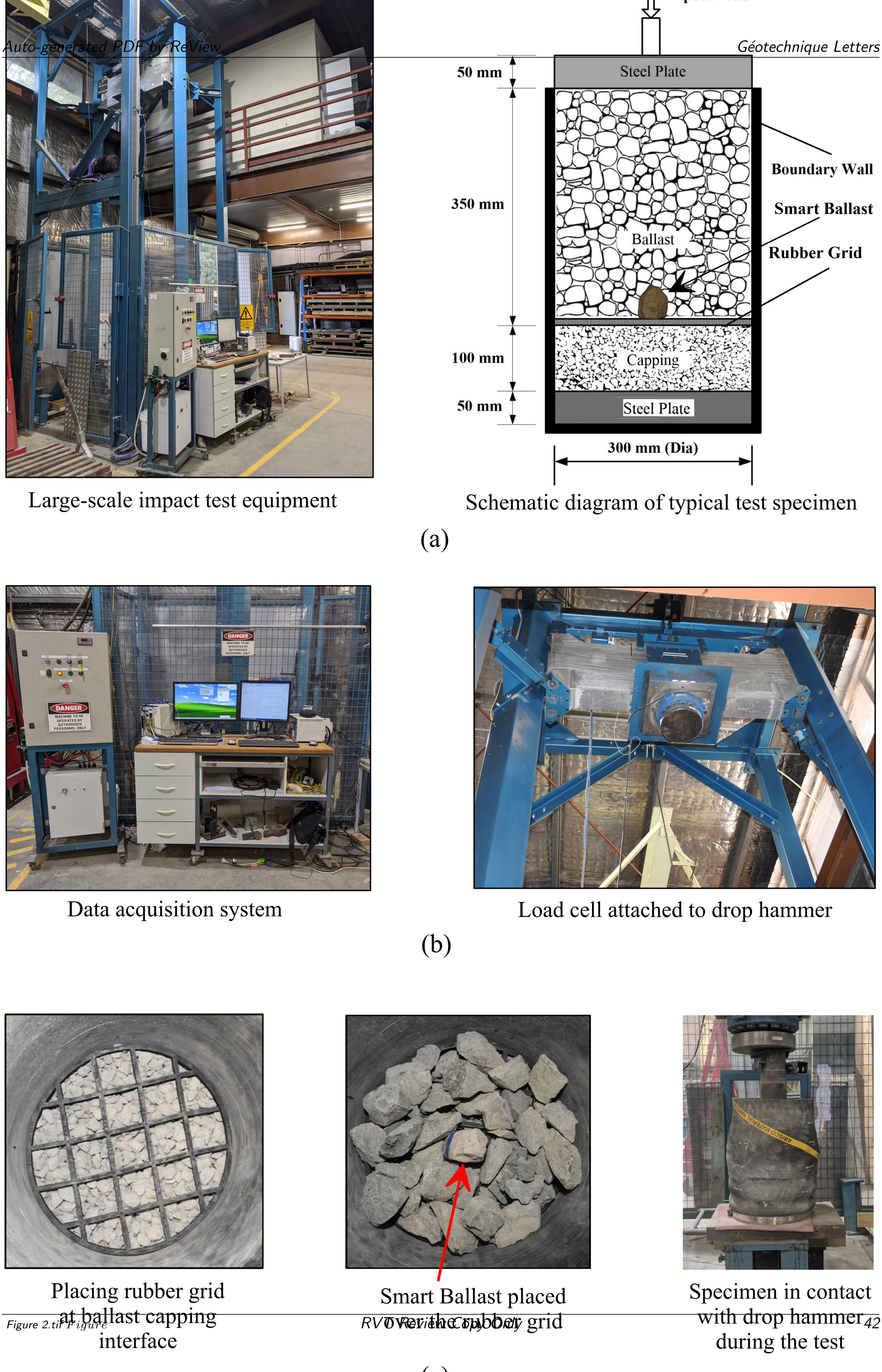
50 mm
Steel Plate
350 mm
Boundary Wall
Smart Ballast
Ballast
Rubber Grid
100 mm
Capping
50 mm
Steel Plate
300 mm (Dia)
DANGER
Large-scale impact test equipment
Schematic diagram of typical test specimen
(a)
Data acquisition system
Load cell attached to drop hammer
(b)
Placing rubber grid at ballast capping interface
Smart Ballast placed over the rubber grid
Specimen in contact with drop hammer during the test

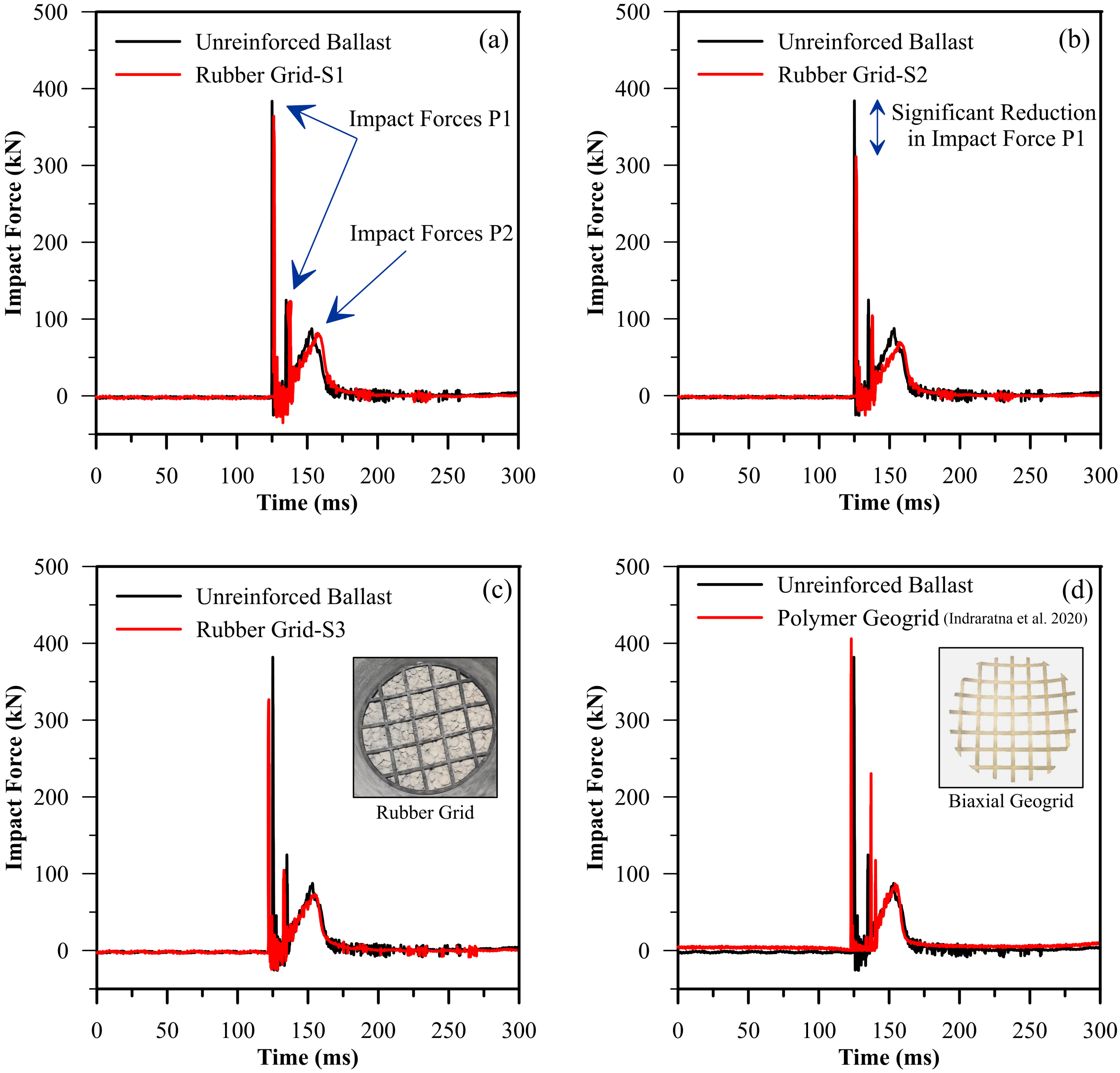

(a)
Unreinforced Ballast
Rubber Grid-S1
Impact Forces P1
Impact Forces P2
Impact Force (kN)
Time (ms)
(b)
Unreinforced Ballast
Rubber Grid-S2
Significant Reduction in Impact Force P1
(c)
Unreinforced Ballast
Rubber Grid-S3
Rubber Grid
(d)
Unreinforced Ballast
Polymer Geogrid (Indraratna et al. 2020)
Biaxial Geogrid

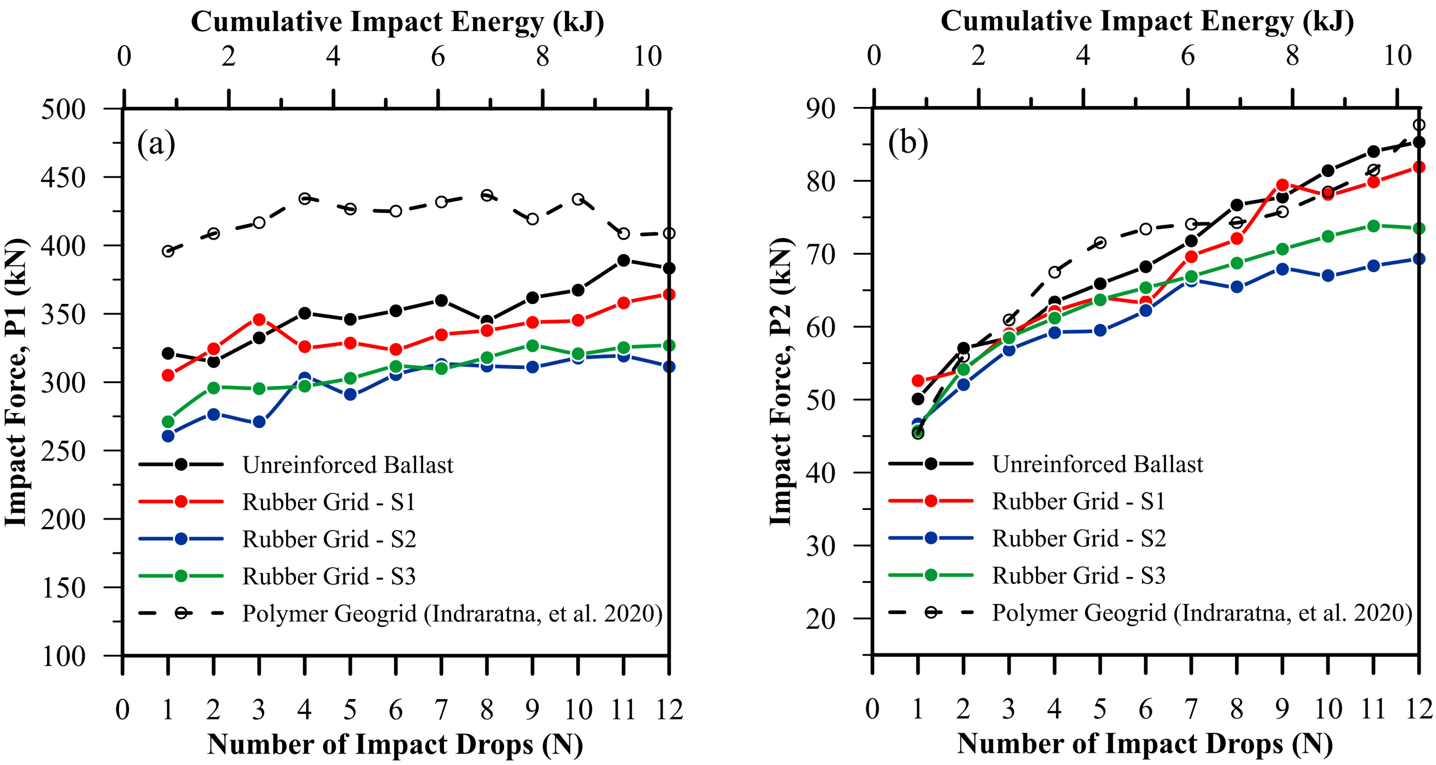
Cumulative Impact Energy (kJ)
0
2
4
6
8
10
(a)
500
450
400
350
300
250
200
150
100
Impact Force, P1 (kN)
Unreinforced Ballast
Rubber Grid - S1
Rubber Grid - S2
Rubber Grid - S3
Polymer Geogrid (Indraratna, et al. 2020)
0 1 2 3 4 5 6 7 8 9 10 11 12
Number of Impact Drops (N)
Cumulative Impact Energy (kJ)
(b)
90
80
70
60
50
40
30
20
Impact Force, P2 (kN)
Unreinforced Ballast
Rubber Grid - S1
Rubber Grid - S2
Rubber Grid - S3
Polymer Geogrid (Indraratna, et al. 2020)
0 1 2 3 4 5 6 7 8 9 10 11 12
Number of Impact Drops (N)

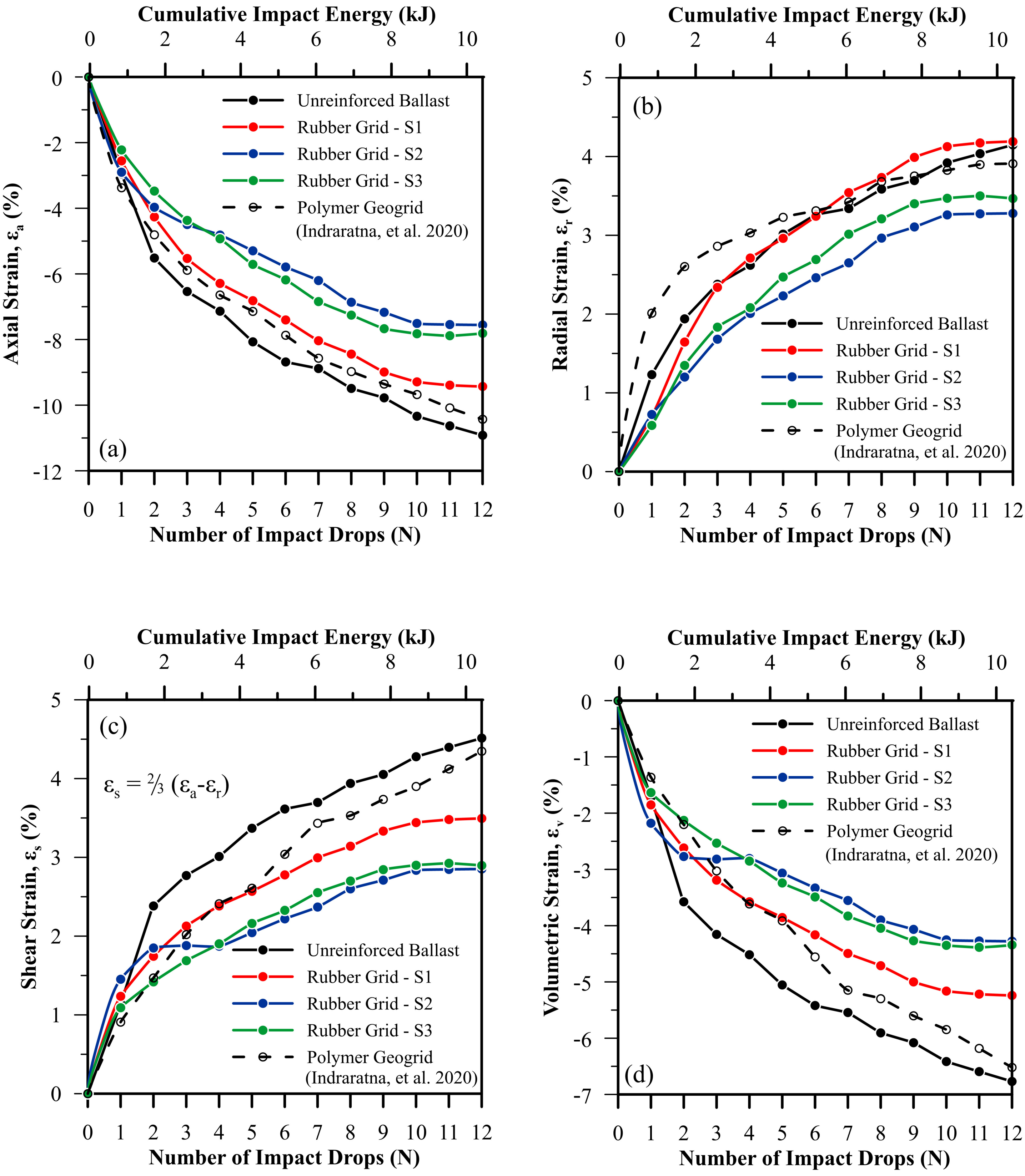
Cumulative Impact Energy (kJ)
Axial Strain, ε_a (%)
Number of Impact Drops (N)
(a)
Unreinforced Ballast
Rubber Grid - S1
Rubber Grid - S2
Rubber Grid - S3
Polymer Geogrid
(Indraratna, et al. 2020)
Radial Strain, ε_r (%)
(b)
Shear Strain, ε_s (%)
(c)
$\varepsilon_s = ⅔ (\varepsilon_a - \varepsilon_r)$
Volumetric Strain, ε_v (%)
(d)

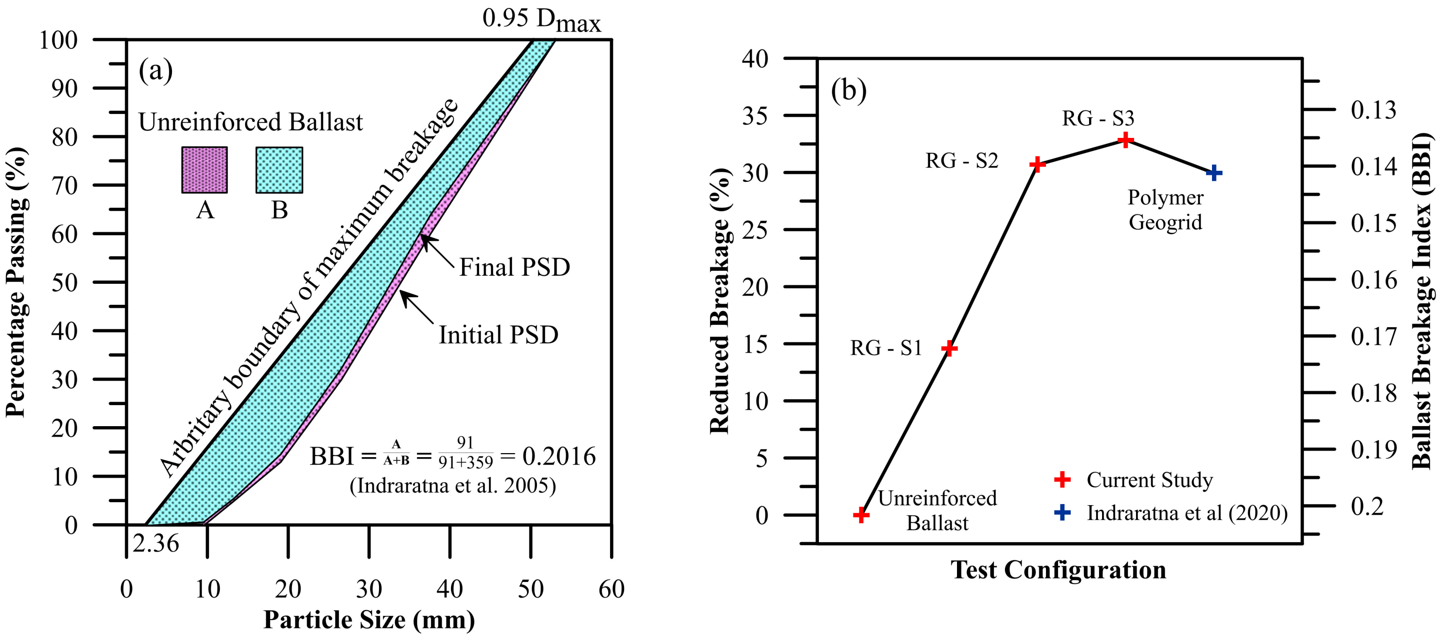
(a)
0.95 Dmax
Unreinforced Ballast
A
B
Arbitrary boundary of maximum breakage
Final PSD
Initial PSD
BBI = A/(A+B) = 91/(91+359) = 0.2016
(Indraratna et al. 2005)
2.36
Percentage Passing (%)
Particle Size (mm)
(b)
RG - S1
RG - S2
RG - S3
Polymer Geogrid
Unreinforced Ballast
Current Study
Indraratna et al (2020)
Reduced Breakage (%)
Ballast Breakage Index (BBI)
Test Configuration

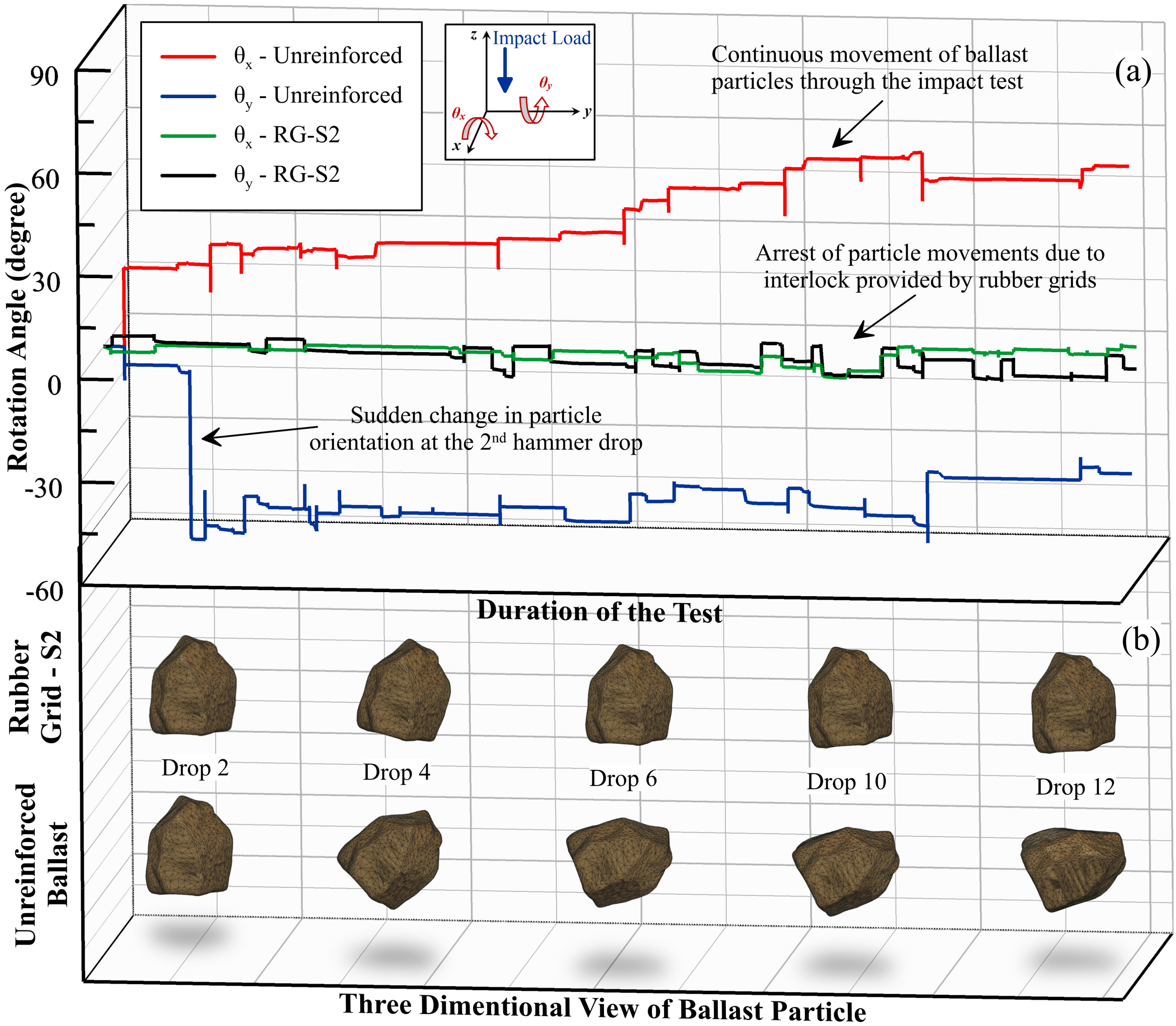

θx - Unreinforced
θy - Unreinforced
θx - RG-S2
θy - RG-S2
Impact Load
z
y
x
θx
θy
Continuous movement of ballast particles through the impact test
(a)
Arrest of particle movements due to interlock provided by rubber grids
Sudden change in particle orientation at the 2nd hammer drop
90
60
30
0
-30
-60
Rotation Angle (degree)
Duration of the Test
(b)
Rubber Grid - S2
Unreinforced Ballast
Drop 2
Drop 4
Drop 6
Drop 10
Drop 12
Three Dimentional View of Ballast Particle

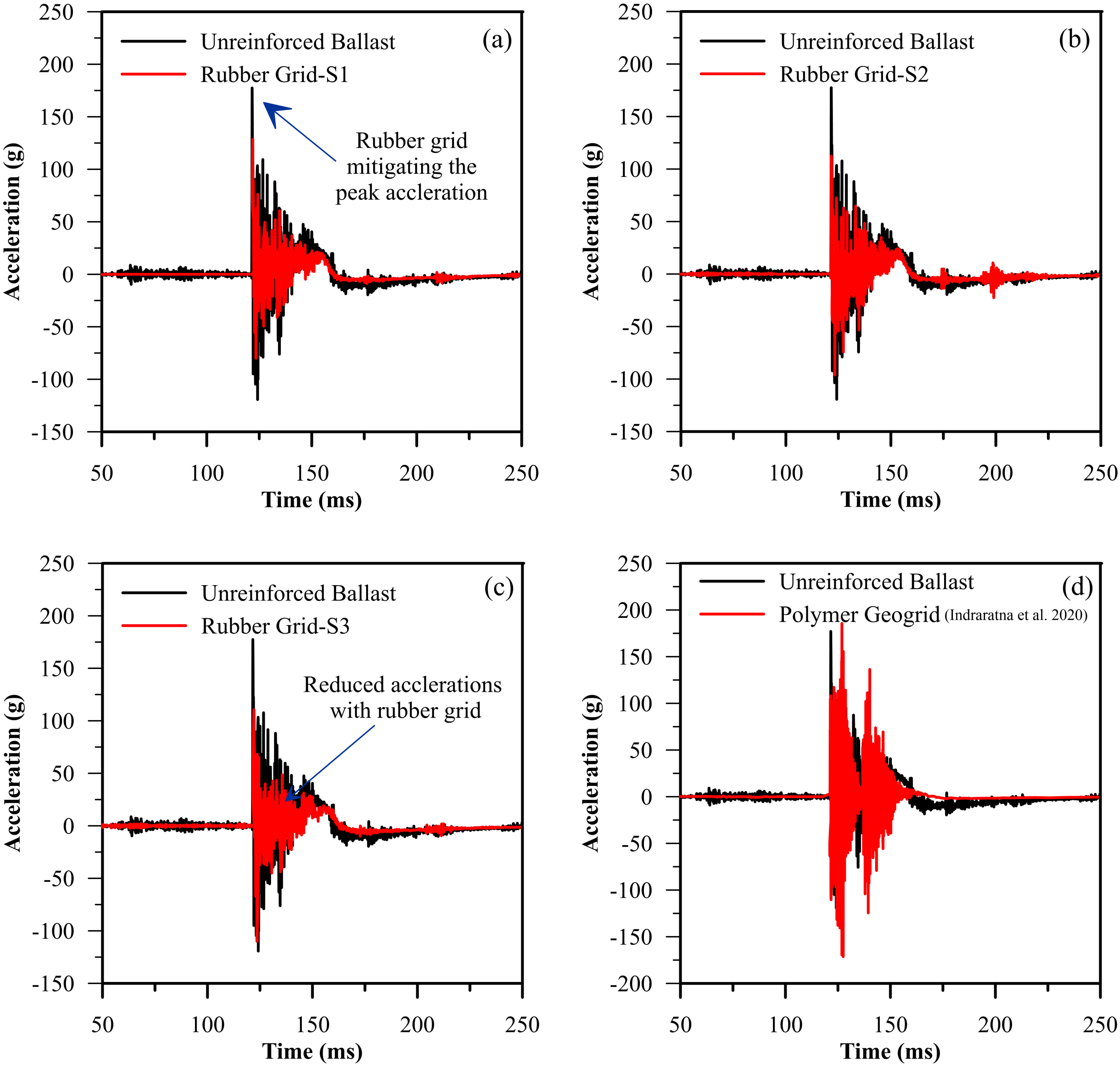

Unreinforced Ballast
Rubber Grid-S1
(a)
Rubber grid mitigating the peak accleration
Acceleration (g)
Time (ms)
Unreinforced Ballast
Rubber Grid-S2
(b)
Unreinforced Ballast
Rubber Grid-S3
(c)
Reduced acclerations with rubber grid
Unreinforced Ballast
Polymer Geogrid (Indraratna et al. 2020)
(d)